Insights into the Effect of Combustion-Generated Carbon Nanoparticles on Biological Membranes: A Computer Simulation Study

Rakwoo Chang

Department of Chemistry, Kwangwoon University, Seoul 139-701, Republic of Korea

Angela Violi*

Department of Mechanical Engineering, University of Michigan, Ann Arbor, Michigan 48109-2125

Received: November 10, 2005; In Final Form: January 12, 2006

Classical molecular dynamics simulations of atomistic models of combustion-generated carbon nanoparticles and lipid bilayers have been performed to explore their possible structural, dynamical, and thermodynamic effects on biological membranes. The DREIDING generic force field is used for the carbonaceous nanoparticles of different morphologies, as produced from combustion sources, and the united atom model was employed for the dimyristoylphosphatidylcholine (DMPC) bilayer. It is observed that particle shape and structure have significant effects on solvation, mobility, adsorption, and permeation behavior of the particles. While combustion-generated carbon nanoparticles with an aspect ratio close to unity prefer to stay near the membrane center, precursors with other shapes mostly reside within the hydrocarbon tail region of the membrane. Carbon nanoparticles are not trapped in a local region even inside the membranes but move freely with a speed depending on their molecular weight. The adsorption of the particles on the surface of the biological membrane is comparable to thermal fluctuations because the weak segregation effect by water molecules is the main driving force to the adsorption behavior. The bigger the precursors are, the stronger they are bound to the membrane surface. The presence of combustion-generated nanoparticles inside the membrane perturbs local lipid density by pushing the neighboring lipid molecules away from the nanoparticles. This, coupled with thermal fluctuations, can induce an instantaneous membrane pore to allow water protrusion. From the umbrella sampling method, the potential of mean force for the permeation of carbona nanoparticles into the bilayer was also obtained. Surprisingly, elongated particles have a free energy barrier an order of magnitude smaller compared with more round ones. In addition, the round carbon nanoparticles showed strong hysteresis due to the local trapping of water molecules. Although the carbon soot precursors studied in this work are not the well-known carbon nanoparticles such as fullerenes or carbon nanotubes, the qualitative features of this study may be applicable to them as well.

I. Introduction

Carbon nanoparticles such as fullerenes, carbon nanotubes, and soot precursors have attracted much scientific and industrial interest regarding their characteristic structural, mechanical, and electric properties.[1−14] For example, their mechanical strength and electrical conductivity due to the delocalization of π bonds have found many applications in nanoscale electrical devices, polymer fillers, fuel cells, cosmetics, and biological sensors.

However, despite the widespread promise of these nanoparticles, especially in new technologies, research on their effect on human bodies and the environment has been rare until recently.[15−23] It is therefore important to assess the potential risk issues associated with nanoparticles, such as exposure, environmental and biological fate, transport, and toxicology.[24] In the environment, the process of combustion is the dominant pathway through which mankind continuously injects particles into the atmosphere at the present time. The most direct and serious risk related to these emissions is the direct absorption of these particles into the living systems of human and animal through the process of respiration, especially in more urban environments. Recent studies[25,26] on the mechanisms by which particles act show that the particle deposition in the epithelial cells in the lung triggers a number of responses: inflammation, production of cytokines that stimulate the release of fibrinogens, which bind to platelets, contribute to their aggregation, and enhance their ability to clot. The high number concentration and small size of nanoparticles lead to high rates of deposition deep in the lung.[27] Ultrafine particles also impair the ability of the macrophage to engulf and remove particles from the extracellular milieu.[28] Therefore, nanoparticles emitted by combustion sources are a very serious health concern because of both their size and the carcinogens with which they are associated.

It is not surprising that combustion-generated carbon nanoparticles may be toxic in respiratory organs such as the lung, considering that it has been known for some time that their allotrope, graphite, can induce pneumoconiosis by inhalation.[29,30] Such carbon nanoparticles have a much larger surface area than graphite, and because of their nanoscale size, they tend to be accumulated in the interior of the body and are not eliminated by the microphage−mucociliary clearance mechanism.[18] However, systematic studies on the toxicity of combustion-generated carbon nanoparticles on lung tissue are absent, although a few

* To whom correspondence should be addressed. E-mail: violi@eng.utah.edu.

10.1021/jp0565148 CCC: $33.50 © 2006 American Chemical Society
Published on Web 02/23/2006

conflicting results have been reported.[17−31] Adelmann et al.[31] reported that fullerenes are no more toxic than quartz powder from the study on the effect of fullerenes on the alveolar macrophages in vitro. Huczko et al.[20,21] also observed that carbon nanoparticles do not show any toxic behavior such as skin irritation, allergy, and lung toxicity. However, in the two recent experiments using mice,[17,18] single-wall carbon nanotubes were found to induce granulomas in the lung unlike graphite, which is much larger in size than carbon nanotubes.

Carbon nanoparticles can also cause serious damage to biological membranes. Sayes et al.[16] recently observed that pure fullerene aggregates (so-called nano- C_{60}), which are weakly soluble in water, kill human cells in culture even at very low concentrations (∼20 ppb). This cytotoxicity tends to decrease over 7 orders of magnitude as more hydroxyl groups are attached to the fullerenes, which enhances their water solubility. It was suggested that the superoxide anions of fullerenes generated in water are responsible for membrane damage and subsequent cell death. However, cumulative experimental and theoretical studies at atomistic length scales are essential to consolidate this postulate.

Due to the recent progress in computational power, it has become routine to study realistic models of biological systems on nanosecond and nanometer scales using molecular dynamics (MD) computer simulations. These simulations provide the atomistic-level information of biological systems under study, which may be difficult to obtain from macroscopic experimental approaches. Such simulations have been successfully applied, for example, to enzyme reactions, protein folding, ion channels, membrane fusion, and so forth.[32−39]

Computer simulation studies for the interaction between carbon nanoparticles and biological materials such as proteins and DNA have also been performed.[40−46] The inhibition of the HIV-1 protease by fullerenes and their derivatives[40,44,45] was studied, and the binding behavior of carbon nanotubes with nucleic acids[42,46] or amylose[41] was also investigated to improve the solubility of nanotubes. Recently, Srinivas and Klein[47] studied the interaction between a synthetic nanotube and a dimyristoylphosphatidylcholine (DMPC) lipid bilayer using the molecular dynamics simulations of a coarse-grained (CG) model.

However, to our knowledge, the computational study on the effect of combustion-generated carbon nanoparticles on biological lipid bilayer membranes using atomistic models has not yet been carried out. This is an important priority considering the possible toxicity of carbon nanoparticles on the biological membranes as described above.

Thus, in this work, we report on the computational investigation of the structural and dynamic effects of combustion-generated carbon nanoparticles on a lipid bilayer using MD simulations of atomistic molecular models. Importantly, combustion-generated carbon nanoparticles produced from combustion sources, rather than well-structured fullerenes and carbon nanotubes, are the primary focus of this study. These nanoparticles, made primarily of carbon and hydrogen, are formed in the initial stage of the soot formation in combustion and later act as seeds for large soot structures. It is generally believed that they are present in considerable abundance from especially diesel and other hydrocarbon emissions.[48,49,50]

This paper is organized as follows. In section II, the molecular models and computer simulation methods used in this study are described in detail. The structural, dynamical, and thermodynamic analyses are then presented in section III, while a summary and conclusions are given in section IV.

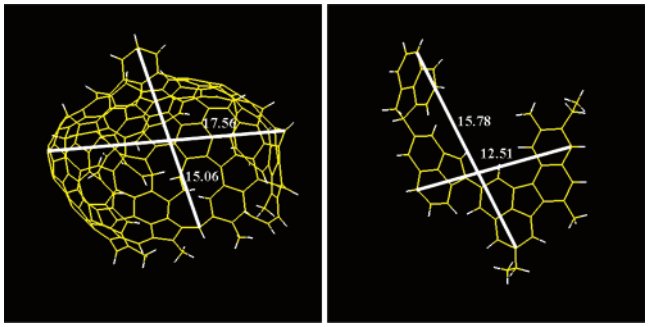


Figure 1. Chemical structures of the combustion-generated carbon nanoparticles investigated in this study. The yellow and white colors correspond to carbon and hydrogen atoms, respectively. The values on the white lines are the distances between carbon atoms in Angstroms.

II. Methods

A. Molecular Models. Combustion-generated carbon nanoparticles with two different morphologies were investigated: a precursor with an aspect ratio close to unity "round" with a formula of $C_{188}H_{53}$ and a precursor with a composition of $C_{50}H_{38}$ "flat" (see Figure 1). The initial configurations of the nanoparticles were obtained using a combination of kinetic Monte Carlo (KMC) and MD methodologies (the atomistic model for particle inception or AMPI code). The AMPI code has been developed to study the transformations that occur in combustion systems during the transition from gas phase to particle inception.[12−14] All dangling bonds of carbon atoms have been hydrogen terminated. Figure 1 shows two representative structures obtained with the AMPI code in different combustion environments. The nanoparticles chosen for this study represent examples of structures found in aromatic and aliphatic flames from the AMPI code. These results in turn correlate with the curvature of carbon layers seen in high-resolution transmission electron microscopy (HRTEM) images of combustion-generated nanoparticles produced in flames that show different curvature of the carbon nanoparticles containing amorphous, graphitic, or fullerenic nanostructure.[51−53]

Both round and flat nanoparticles have the size of around 17 Å in the longest dimension. The round precursor consists of a network of five- to eight-membered fused rings such as buckyballs, whereas the flat one has four planar aromatic moieties connected by freely rotating bonds. The force fields for those carbon nanoparticles were generated automatically using a utility in the molecular dynamics simulation package DL_POLY,[54] which searches all possible bonding, angle, dihedral, and inversion potential sets for a given hydrocarbon configuration and assigns the corresponding DREIDING force field[55] to each potential. The DREIDING force fields are generic force fields for "nonmetallic" main-group elements (such as C, N, and O) plus H and a few metals (Na, Ca, Zn, and Fe). To use a significantly long simulation time step, all bond pairs were constrained by using SHAKE.[56]

The molecular model of biological membranes used in this study is the united atom model of DMPC lipid bilayer membranes,[57] which has been used extensively and successful in MD studies.[58−65] The DMPC bilayer membrane, which consists of 64 DMPC lipids, is about 34 Å thick and, therefore, the sizes of the two carbonaceous nanoparticles are comparable to the thickness of one leaflet. A total of 2000 water molecules were also included in the simulation using the TIP3P model.[66]

The membrane size used in this study is relatively small compared to the recent membrane simulations.[67−70] However, many computer simulations of membrane systems have been

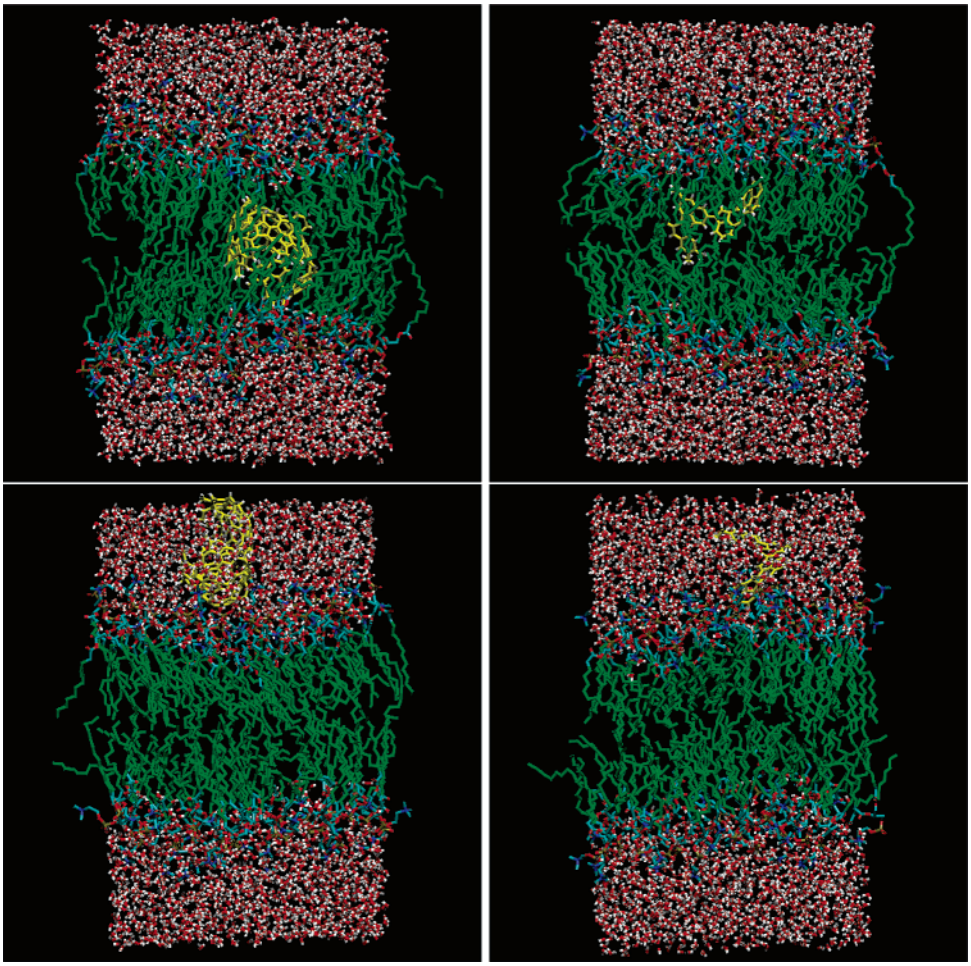


Figure 2. Representative snapshots of the four systems examined in this study.

performed with the similar size and length to our simulations, and many interesting structural thermodynamics insights have been gained from those studies. Previous studies[32,65] showed that the membrane systems of several nanometers in size can reproduce most of the structural properties observed in experiments such as pair correlation, order parameter, density profile, and so forth, except for very long-ranged membrane motions such as undulation.

In addition, since the longest dimension of the combustion-generated carbon nanoparticles used in this study is at most 17 Å, the lateral dimension of the membrane is around 2.4 times bigger than the nanoparticles. Please notice that carbonaceous nanoparticles do not possess any electric charges or dipoles, the interactions of which are long ranged: that is, the interactions between the nanoparticles and between the nanoparticles and lipids or water molecules are mainly the short-ranged van der Waals (vdW) interaction. This short-range character of the interactions of the nanoparticles is also seen from the two-dimensional (2D) pair-correlation function between the centers of masses of the nanoparticles and DMPC lipids, which has been newly added to the paper. Therefore, we believe that the finite size effect of our simulation results is not significant.

The initial configurations of the carbonaceous nanoparticle−membrane systems were generated as follows. First, an artificial point atom was inserted at a position where the precursor should be located inside or outside an equilibrated bilayer system. Next, the radius of the phantom atom (or the Lennard-Jones parameter σ) was gradually increased with a very small time step until the hole grows big enough to accommodate the nanoparticle. Then, the artificial atom was replaced by the precursor, and the resulting configuration was equilibrated until there was no drift in simulation cell dimensions and thermodynamic quantities, such as total energy, pressure, and surface tension.

B. Molecular Dynamics Simulations. 1. Equilibrium MD Simulations. Figure 2 shows the four carbonaceous nanoparticles−membrane systems that are analyzed in this work: round and flat particles inside and outside the DMPC membrane. For each nanoparticle−membrane geometry, two independent configurations were generated and equilibrated using the MD simulations of the $NP_z\gamma T$ ensemble, where N represents the total number atoms in the simulation, P_z is the z-component of the pressure tensor, which was set to 1 bar, γ is the membrane surface tension, set to 0 N/m, and T is the system temperature, set to 308 K in this study. The MD simulations were performed in DL_POLY 2.14 modified for the $NP_z\gamma T$ ensemble. Details of the DMPC membrane model can be found elsewhere.[65] The simulation cell dimensions for all cases were around 46 Å × 41 Å × 70 Å irrespective of the locations or the morphology of the carbonaceous nanoparticles.

For each carbon nanoparticle−membrane configuration, 10 ns equilibrated trajectories were saved every 1 ps and used for further analysis. The results shown in this paper are the averages of the two independent 10 ns trajectory runs for each case.

2. Umbrella Sampling. To study the permeation behavior of carbon nanoparticles into lipid bilayer membranes, the umbrella sampling method[71] was implemented, by which the potential of mean force (or the free energy) can be obtained along a reaction coordinate for the process of interest. More details about the method used here can be found elsewhere.[72]

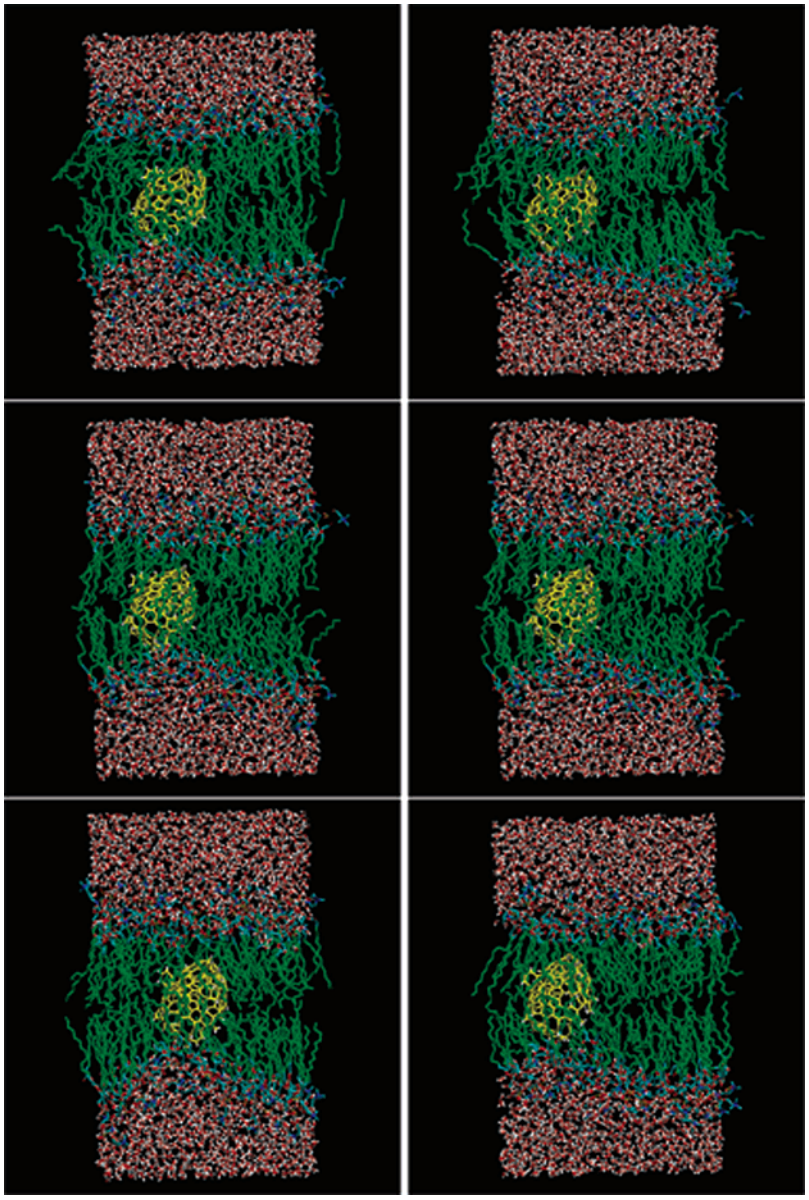


Figure 3. Snapshots of the round nanoparticle inside the membrane bilayer taken every 2 ns.

The reaction coordinate ξ was chosen as the *z*-directional distance between the center of mass of the nanoparticle and the membrane center. In this method, a biased potential is additionally applied in the original molecular dynamics routine to confine the system within a small window of the reaction coordinate. In the present work, a harmonic potential, U_{umb}, with the spring constant, k_{umb}, of 10 kcal/(mol·Å^2) was used

$$U_{umb} = \frac{1}{2} k_{umb}(\xi - z_{win})^2 \tag{1}$$

where

$$\xi = \frac{\sum_{i,\text{nanoparticle}} m_i z_i}{\sum_{i,\text{nanoparticle}} m_i} - \frac{\sum_{j,\text{membrane}} m_j z_j}{\sum_{j,\text{membrane}} m_j} \tag{2}$$

m_i is the mass of the *i*th atom, and z_{win} is the center of each window.

The initial configuration of the carbon nanoparticle−membrane system in each window was obtained by pulling the nanoparticle from an equilibrated configuration in the neighboring window (0.5−1.0 Å apart) using U_{umb}. A total of 1 ns MD trajectories was collected in each window, and the initial 50 ps of the trajectories was discarded for equilibration. The remaining 950 ps equilibrated trajectories were used to calculate the potential of mean force (pmf) profile for a narrow range of ξ within each window.

For the round nanoparticle system, 121 windows were employed at 0.25 Å intervals, spanning from $\xi = 0$ Å to 30 Å; for the flat one, a total of 209 windows at 0.125 Å intervals, spanning from $\xi = 0$ Å to 26 Å, were used.

The free energy profile (or pmf) for the whole range of the reaction coordinate was obtained by assembling each free energy profile in each window using the weighted histogram analysis method (WHAM).[72]

III. Results and Discussion

A. Behavior of Combustion-Generated Carbon Nanoparticles near Lipid Bilayers. Snapshots of the round nanoparticle residing inside the DMPC bilayer membrane were taken every 2 ns and are shown in Figure 3. Although the DMPC lipid

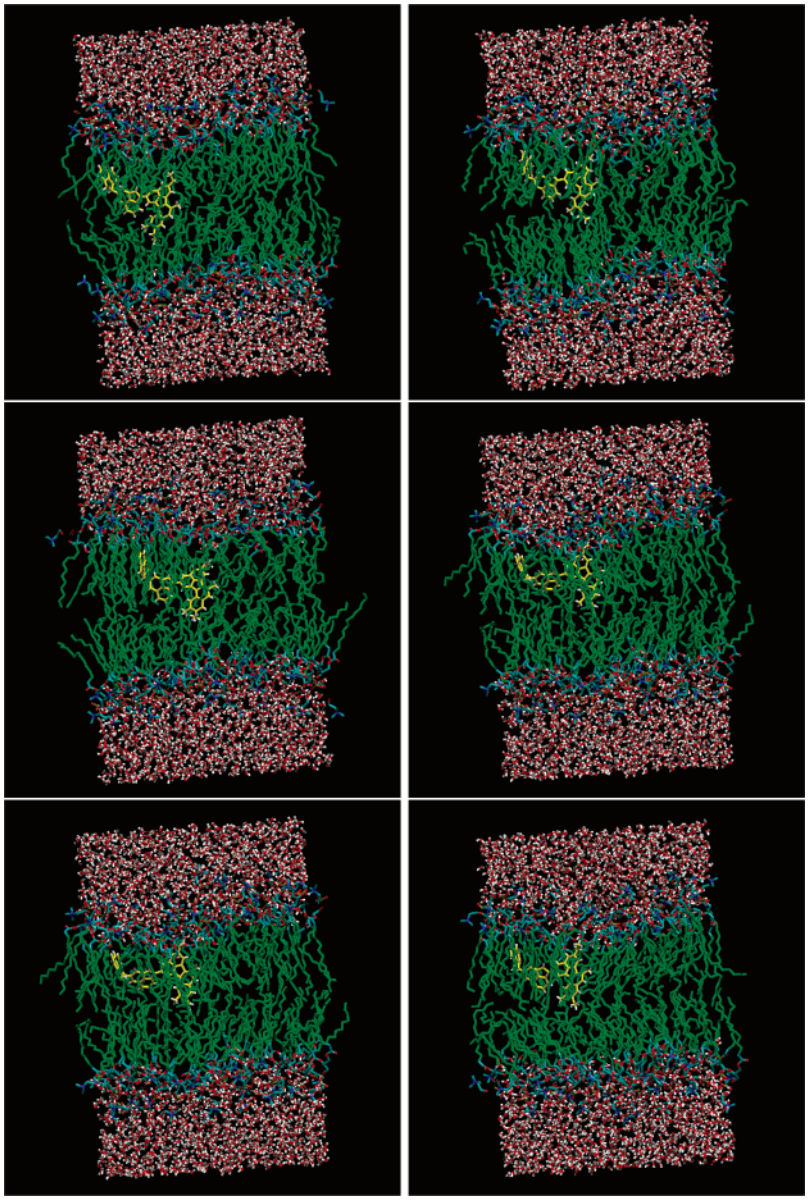


Figure 4. Snapshots of the flat nanoparticle inside the membrane bilayer taken every 2 ns.

configurations change significantly, the carbon nanoparticle does not seem to change its position much and almost looks trapped in a local membrane region. As will be shown later in the text, this is not true and in fact the nanoparticle still moves, although its diffusion is much slower than that of single DMPC lipids. However, the particle spends most of the simulation time at the membrane center, and the membrane region where the particle resides is slightly smaller in thickness, so that several water molecules protrude into the membrane toward the nanoparticle. This behavior will be discussed in detail in section 3.2.

Unlike the round precursor, the flat nanoparticle resides preferentially in the hydrocarbon tail regime rather than in the membrane center, the snapshots of which are seen in Figure 4. This behavior is also observed and confirmed by the density profile and the pmf profile, which will be presented later. In the case of the flat particle precursor, it is also noticeable that the nanoparticle changes its own conformation quickly and moves much faster than the round one.

During the 10 ns simulation used for each system, both the carbon nanoparticle and the membrane retained stable structures without showing any signature of breakage, although there is an indication of instantaneous membrane pore formation. However, it should also be noted that the stability of the lipid bilayer membrane is enforced by the periodic boundary conditions in the computer simulations.[65]

In Figure 5, the snapshots of the round nanoparticle located outside the membrane are reported every 2 ns. Water molecules were omitted for clarity. Since the carbon soot precursor is hydrophobic, it is pushed away from the water region toward the membrane and the trimethylamine groups, in the headgroups of the DMPC lipids, stick out from the membrane to support the nanoparticle. However, as shown in Figure 5, the round soot precursor moves fast by tumbling relatively freely from one region of the membrane−water interface to another, compared with the situation where it is located inside the membrane. In addition, from the distance fluctuations between the nanoparticle and the membrane headgroup interface in the snapshots, the carbon nanoparticle does not look strongly bound to the membrane.

Whether carbon nanoparticles would be adsorbed onto biological membranes or float around in the water phase is related to the subtle balance of various forces, such as nanoparticle−water and nanoparticle−membrane interactions, as well as the entropic effects of water molecules. Since the

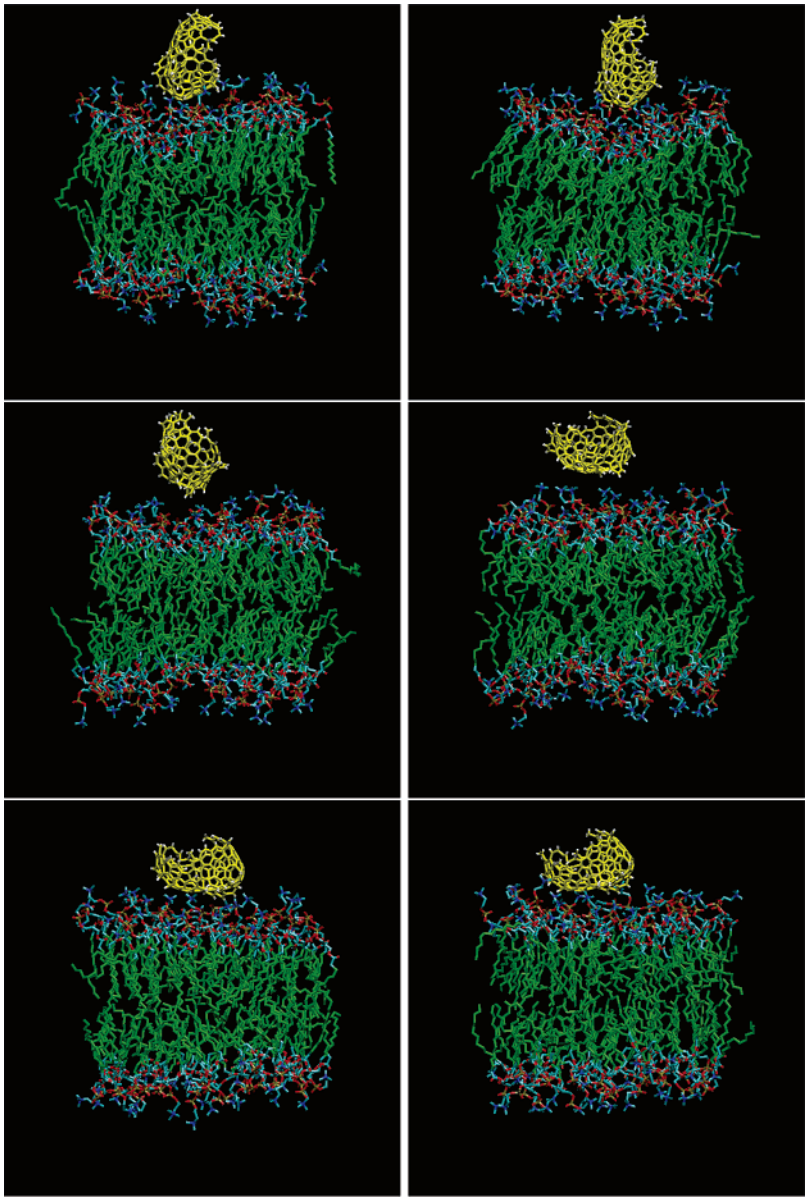


Figure 5. Snapshots of the round nanoparticle outside the membrane bilayer taken every 2 ns. Water molecules are omitted for clarity.

lipid headgroups are also hydrophilic, there would not be much energetic advantage in shifting carbon nanoparticles from the water phase to the water−membrane interface. Therefore, this weak adsorption of the carbon nanoparticles indicates that the entropic gain, by pushing the nanoparticle toward the membrane, is comparable to the thermal fluctuations. Since this entropic gain is diminished with smaller carbon nanoparticles, the adsorption of the flat particle is expected to be weaker than that of the round one.

The morphology of carbon nanoparticles has significant effects on their dynamics as well. Figure 6 shows the mean square displacements (MSDs) of carbon nanoparticles and a single DMPC lipid in the direction parallel ($\langle DR_x^2 + \Delta R_y^2\rangle/4$) or normal ($\langle DR_z^2\rangle/2$) to the bilyer plane. It should be noted that the DMPC MSDs were averaged over the two nanoparticle systems and generally, the lipid diffusion was faster in the presence of the flat carbon nanoparticle than the round one. Inside the membrane, as shown in Figure 6a, the flat nanoparticle moves as fast as single DMPC lipids, whereas the diffusion of the round soot precursor is around half the value of the flat one in both parallel and normal to the membrane directions. This is not surprising because the mass of the flat particle (638 g/mol) is similar to that of the DMPC molecule (678 g/mol) and the round nanoparticle (2309 g/mol) is more than three times heavier than the lipid molecule. However, the important point is that these carbon nanoparticles can still move considerably inside the membranes.

This situation changes dramatically when the carbon nanoparticles are located in the membrane−water interface, which is shown in Figure 6b. Although the round particle diffuses at the same speed as single DMPC lipids, the flat particle diffuses more than three times faster than the round one in the direction parallel to the membrane plane. For reference, the diffusion of single water molecules is around 20 times as fast as that of the flat nanoparticle. The diffusion in the direction normal to the membrane plane shows the same behavior: the diffusion of the flat nanoparticle is much faster than that of the round one or single DMPC lipids. This strongly suggests that the flat particle floats around in the water phase, and it is not much adsorbed on the membrane surface, which is consistent with the previous argument about the entropic effect on the nanoparticle adsorption.

The diffusion coefficient of each species can be obtained from the slope of the corresponding MSD curve. By the use of only

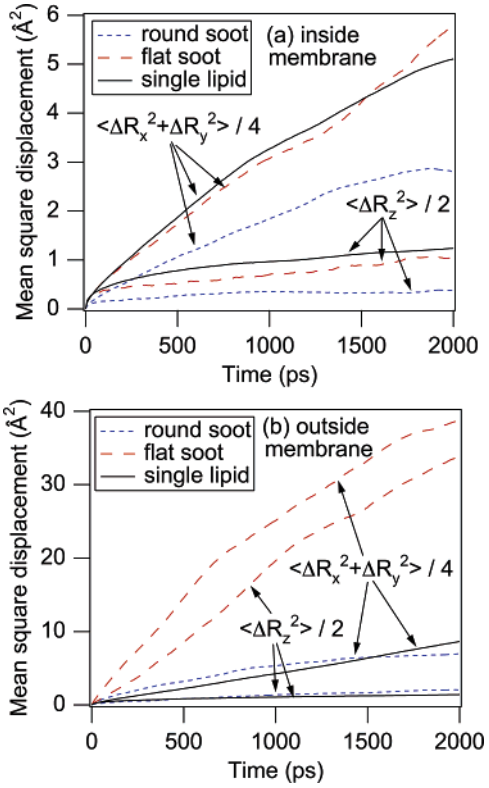


Figure 6. MSDs of carbonaceous nanoparticles and a single DMPC lipid in the direction parallel ($\langle DR_x^2 + \Delta R_y^2\rangle/4$) or normal ($\langle DR_z^2\rangle/2$) to the membrane plane when the carbon nanoparticles are located (a) inside or (b) outside the membrane.

the 1−2 ns MSD data, it is found that the diffusion coefficients of the DMPC molecules in the direction parallel to the membrane plane are $(1.96 \pm 0.11) \times 10^{-3}$ and $(4.40 \pm 0.20) \times 10^{-3}$ Å^2/ps when the carbonaceous nanoparticles are located inside and outside the membrane, respectively. So, carbon nanoparticles also hinder the motion of the surrounding lipid molecules inside the membrane.

B. Membrane Breakage Induced by Carbon Nanoparticles. It has been speculated that carbon nanoparticles can kill human cells by the oxidative damage on the membrane.[16] In this work, we have found a different signature of membrane damage caused by the carbon nanoparticles, which is attributed to a physical process. The physical membrane damage we have observed is the instantaneous formation of a pore in the lipid bilayer membrane as induced by the carbon nanoparticles. In Figure 7a, we show a snapshot of the round particle present inside the DMPC bilayer membrane. Although the size of the carbonaceous nanoparticles is comparable to the thickness of one leaflet of the membrane, the round particle stays at the membrane center most of the time. Water molecules within 5 Å from the carbon particle are depicted as vdW spheres. The membrane region around the nanoparticle forms a pore instantaneously to allow water protrusion. When we measure the lipid density around the carbonaceous nanoparticle, it is observed that the membrane region right above (or below) the nanoparticle is deficient in lipid molecules. This deficiency coupled with the thermal fluctuation induces the formation of a pore. This local breakage of the lipid bilayer membrane could lead to a larger pore formation in the presence of lateral membrane tension.

A similar behavior is also seen in Figure 7b, where the flat particle residing inside the membrane is exposed to several water molecules from the water region. In this case, the pore is formed more easily because the nanoparticle stays in one leaflet of the bilayer membrane preferably.

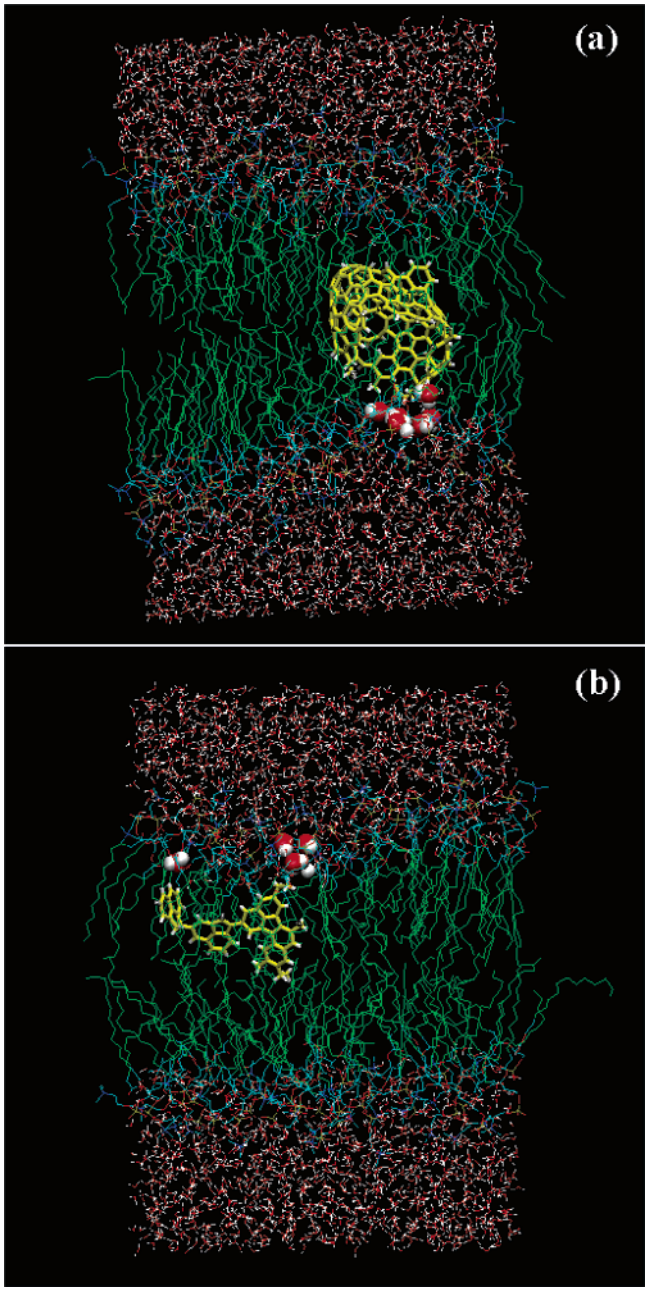


Figure 7. Water molecules within 5 Å of a carbon nanoparticle are depicted as van der Waals spheres: (a) round nanoparticle and (b) flat nanoparticle.

This nanoparticle-induced pore formation is also seen from the 2D pair-correlation function, $g_{2D}(r)$, between the centers of masses of the nanoparticle and DMPC lipids, as shown in Figure 8. Although the uncertainty is large, it is clear that the DMPC lipids are depleted up to 4 Å in case of the round nanoparticle. This correlation along with a second dip around 8 Å goes up to 10 Å, which is reasonable considering the size of the carbon nanoparticle. This again verifies the use of the moderate size of membrane in this study. This strong correlation is not however clearly seen in case of the flat nanoparticle. This may be because the flat particle is well adapted in the hydrocarbon tail region of the lipids without perturbing the lipid structure significantly.

One might question that the pore formation induced by the carbon nanoparticles should be preceded by the permeation of

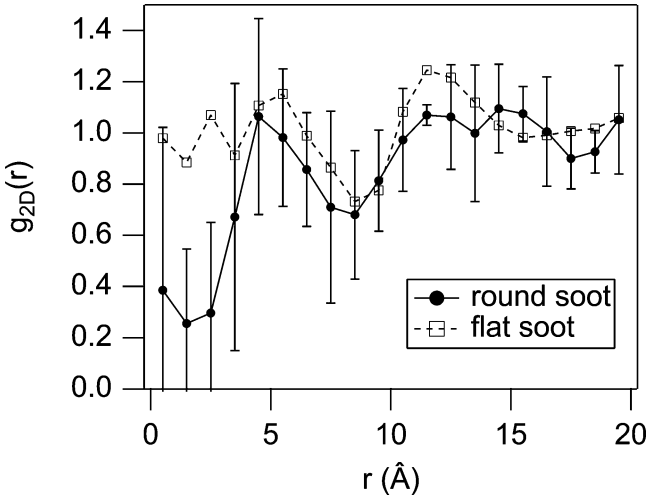


Figure 8. 2D pair-correlation functions, $g_{2D}(r)$, between the centers of masses of the carbon nanoparticles and DMPC lipids. The error bars for the flat nanoparticle are comparable to those for the round ones and are omitted for clarity.

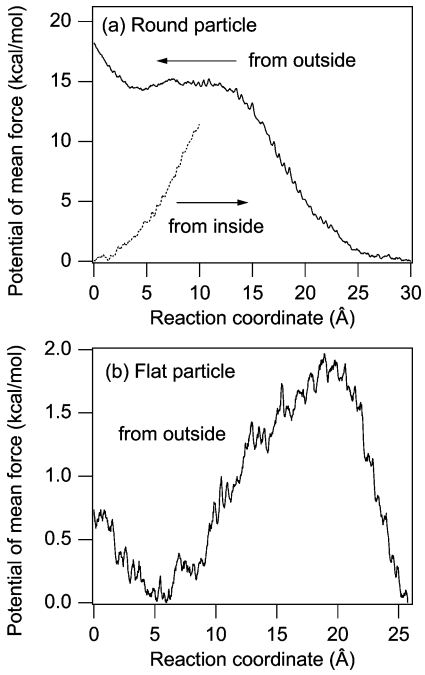


Figure 9. Potential of mean forces (pmf's) for the permeation of (a) the round and (b) the flat carbon nanoparticles. The pmf of the round nanoparticle shows severe hysteresis. The reaction coordinate (ξ) is the *z*-directional distance between the center of masses of the nanoparticle and the lipid bilayer membrane.

the nanoparticle into the membrane. If the permeation is a very slow process, the membrane breakage by the nanoparticles may be less of a concern. To address this issue, we have calculated the pmf for the permeation process and present the results in the next section.

C. Permeation of Carbon Nanoparticles into the Membrane. The pmf of the permeation of carbon nanoparticles into the DMPC bilayer was calculated using the umbrella sampling technique described in the Methods section.[71] The calculated pmf's as a function of reaction coordinate ξ are shown for the round and the flat nanoparticles, respectively, in Figure 9.

Similar to the diffusion of carbon nanoparticles, which depends strongly on particle morphology, the permeation behavior is also highly affected by the morphology and structure of the carbon nanoparticles. When the round particle was

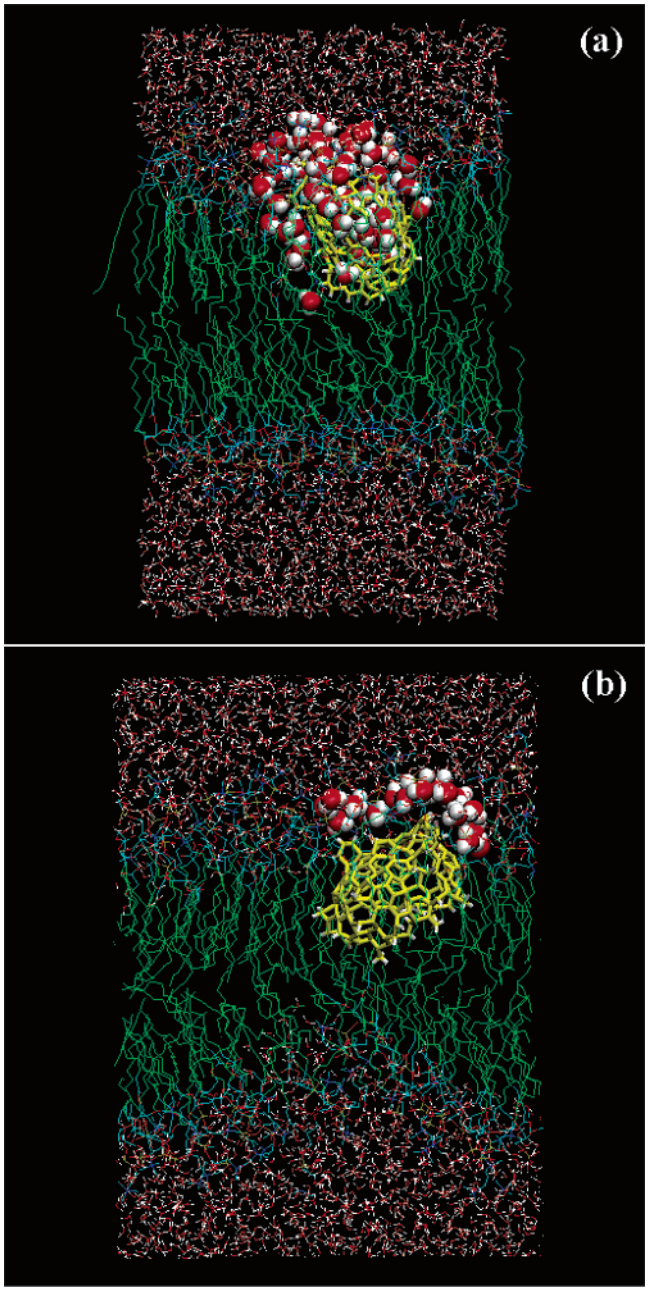


Figure 10. Snapshots from Figure 8a at $\xi = 10$ Å. The round nanoparticle was pulled from (a) outside or (b) inside the membrane using an umbrella potential.

initially pulled from the membrane−water interface toward the membrane center by a harmonic umbrella potential and the resulting configuration was used for the umbrella sampling (the solid line in Figure 9a), the pmf obtained shows a large energy barrier (~15 kcal/mol) increasing from $\xi = 20$ Å up to $\xi = 13$ Å, followed by a plateau regime between $\xi = 13$ Å and 5 Å. After the pmf reaches a minimum around $\xi = 5$ Å, it starts rising steeply again until $\xi = 0$ Å. Considering the thermal energy is around 0.6 kcal/mol, this energy barrier is too high for the round nanoparticle to penetrate the membrane only by thermal fluctuations.

In principle, the pmf along the reaction coordinate should not rely on the way or direction the sampling is performed. However, the pmf profile looks completely different when the initial configurations for the sampling were prepared from the nanoparticles located inside the bilayer membrane, which is shown as a dotted line in Figure 9a. In this case, the pmf strongly

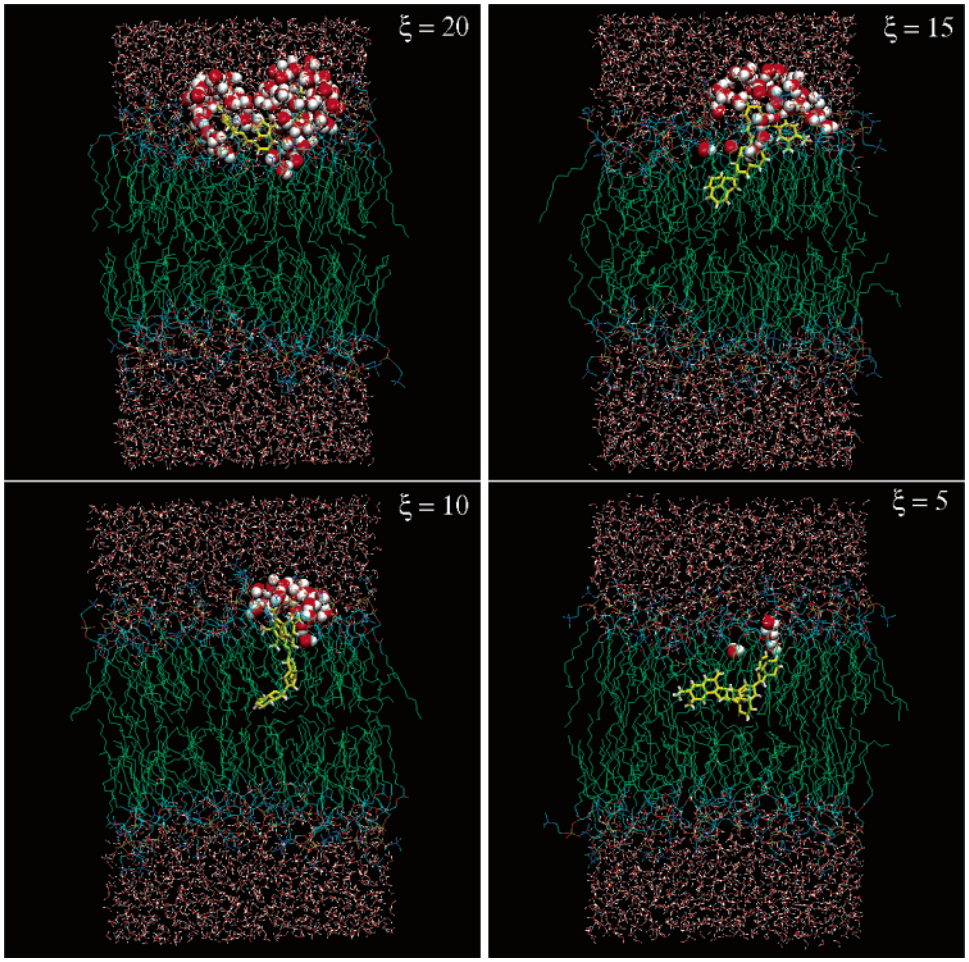


Figure 11. Snapshots from Figure 8b at $\xi = 20$, 15, 10, and 5 Å. The flat nanoparticle was pulled from outside the membrane using an umbrella potential.

increases from $\xi = 0$ Å until $\xi = 10$ Å without showing any minimum or plateau.

The origin of this hysteresis can be understood by looking at snapshots taken at $\xi = 10$ Å for the round nanoparticle and reported in Figure 10. The snapshots were taken from the equilibrated configurations at $\xi = 10$ Å when the nanoparticle was initially located (a) outside and (b) inside the bilayer membrane, respectively. When the nanoparticle is initially pulled from the membrane−water interface, the surrounding water molecules accompany the carbonaceous nanoparticle all the way to the center of the membrane. Therefore, the large energy cost resulting from the hydrophobic mismatch between water and hydrocarbon tails contributes to the large free energy barrier for the permeation process of the carbon nanoparticles. Another contribution is the energy cost of forming a membrane pore with the diameter of around 17 Å for the entrance of the precursors.

On the other hand, when the carbonaceous nanoparticle is initially located inside the bilayer and pulled toward the membrane−water interface, no water molecules are present around the nanoparticle until the nanoparticle has reached the membrane−water interface. This difference in the water arrangement is the source of the large hysteresis between the two paths. One might narrow the gap by sampling the trajectory for much longer than a nanosecond to make water molecules rearrange themselves around the nanoparticle, but this will be too costly even with the current state-of-the-art computing resources. These results clearly show that the round-shaped nanoparticle is stable in the bilayer, but the mechanism for its insertion is not known. Future research will be developed to establish this mechanism.

The pmf for the flat nanoparticle is very different from that of the bigger round soot precursor as seen in Figure 9b. Unlike the round nanoparticle, the pmf for the flat particle shows a small peak (2.0 kcal/mol), around $\xi = 20$ Å, where the headgroups of the DMPC lipids are located. The reason the flat nanoparticle has such a low permeation energy barrier compared to the round one can be understood by looking at the snapshots taken at $\xi = 20$, 15, 10, and 5 Å in Figure 11. Although the flat particle was initially pulled from the membrane−water interface, there is no water surrounding the nanoparticle except near the interface. This implies that water molecules having originally surrounded the carbonaceous nanoparticle can easily leave it on a nanosecond time scale when the soot precursor starts to insert into the membrane. This is related to the morphology of the flat soot precursor: that is, when it starts to enter the membrane, the planar moiety of the soot precursor is tilted to make it perpendicular to the membrane plane (see parts a−c of Figure 11). This rearrangement of the carbonaceous nanoparticle allows the water to escape more easily from the nanoparticle region. Once the flat particle arrives at the hydrocarbon region, it rearranges itself again to minimize the contact energy (see Figure 11d).

The small free energy barrier of $3-4k_BT$ allows the flat nanoparticle to permeate into the membrane on the picosecond time scale, as can be approximated from a simple transition state theory ($k = (k_BT/h)\exp(-\Delta G^{\ddagger}/RT)$).[73] However, during the two independent 10 ns molecular dynamics simulations, no

permeation process was observed. This inconsistency can be explained by the fact that the free energy profile was obtained assuming the structural relaxation orthogonal to the reaction coordinate, which includes the relaxation of membrane motions, is fast compared to the nanoparticle permeation process. However, the membrane motions have various long-range hydrodynamic modes such as bending, protrusion, and lateral expansion (or contraction).[74] In particular, the nanoparticle permeation is strongly coupled to the membrane area expansion, the modulus of which is around 0.145 N/m.[75] Therefore, it is mostly likely that, when a nanoparticle tries to get into the membrane, it will feel a nearly static membrane configuration at long length scales and in most cases, the attempt will not be successful by the unfavorable membrane geometries. However, the conclusion is still valid that flat nanoparticles are likely more able to penetrate into the biological membranes than the round particle.

The small peak in the pmf of the flat particle is followed by a local minimum around $\xi = 5$ Å, not at the membrane center ($\xi = 0$ Å). This behavior was also seen from the snapshots (Figure 4). That is, the flat nanoparticle prefers to reside near the hydrocarbon side chain regime to the membrane center. This is also a consequence of the morphology of the carbon nanoparticles. Since the flat particle does not provide mirror-plane symmetry but instead a bent structure, the membrane center region does not give any energetic benefit to the nanoparticle. In addition, the leaflike structure can be easily adapted to the lipid region, not causing much steric hindrance.

IV. Summary and Conclusions

In this work, classical molecular dynamics simulations have been performed for atomistic models of combustion-generated carbon nanoparticles and DMPC lipid bilayers to study their structural, dynamical, and thermodynamic effects on the biological membranes. Particle morphology has significant effects on structure, mobility, adsorption, and permeation behavior of the particles. While round nanoparticles prefer to stay near the membrane center, flat ones mostly reside in hydrocarbon tail regions of the DMPC lipids. Carbon nanoparticles are not trapped in a local region even inside the biological membranes but move freely with reduced speed depending on their molecular weight. The adsorption of carbon nanoparticles on the surface of the biological membrane is comparable to thermal fluctuations because the weak segregation effect by water molecules is the main driving force to the adsorption behavior. The bigger the carbon nanoparticles are, the stronger they are bound to the membrane surface. The presence of carbon nanoparticles inside biological membranes perturbs the local lipid density by pushing the lipid molecules away from the precursors. This, coupled with thermal fluctuations, induces an instantaneous membrane pore to allow water protrusion.

The pmf's for the permeation of carbon nanoparticles into the lipid bilayers were calculated using the umbrella sampling method. Surprisingly, flat nanoparticles have an order of magnitude smaller free energy barrier compared with round particles. In addition, the round nanoparticle shows strong hysteresis due to the local trapping of water molecules. Although the pmf of permeation by the flat nanoparticle shows a free energy barrier of just $3-4k_BT$, the permeation process was not observed during multinanosecond computer simulations. This indicates that the pmf along a simple reaction coordinate defined by the distance of the nanoparticle to the bilayer center should be used with caution. Additional coordinates may be important to the nanoparticle permeation process, and this will be explored in the future.

It will also be interesting to study the collective effects of combustion-generated carbon nanoparticles either inside the membrane or on the membrane surface because fullerenes usually form water-soluble aggregates in solution.[16] In addition, the effect of chemically modified carbon nanoparticles on biological membranes is another research subject of interest. One caveat to this work is that we did not implement any chemical features such as radical formation and oxidation, which is suspected to be a main source of the membrane damage by carbon nanoparticles. It will be desirable in the future to carry out quantum chemical calculations on these systems, although there is some ambiguity as to how to set up the quantum mechanical region.

The current work will hopefully promote more experimental and theoretical studies on the toxic effect of carbon nanoparticles and their role in human health.

Acknowledgment. We thank Professor G. A. Voth of the University of Utah for his support and encouragement during the early stages of this project. Some of the computational resources have been provided by the National Institutes of Health (NCRR 1 S10 RR17214-01) on the Arches Metacluster, administered by the Center for High Performance Computing at the University of Utah. The present research has also been supported by the Research Grant of Kwangwoon University in 2005 to R.C.

References and Notes

(1) Ajayan, P. M.; Charlier, J. C.; Rinzler, A. G. *Proc. Natl. Acad. Sci. U.S.A.* **1999**, *96* (25), 14199−14200.

(2) de Jonge, N.; Bonard, J. M. *Philos. Trans. R. Soc. London, Ser. A* **2004**, *362*, 2239−2266.

(3) Dresselhaus, M. S.; Dai, H. *MRS Bull.* **2004**, *29* (4), 237−239.

(4) Lin, Y.; Taylor, S.; Li, H. P.; Fernando, K. A. S.; Qu, L. W.; Wang, W.; Gu, L. R.; Zhou, B.; Sun, Y. P. *J. Mater. Chem.* **2004**, *14* (4), 527−541.

(5) Bosi, S.; Da Ros, T.; Spalluto, G.; Prato, M. *Eur. J. Med. Chem.* **2003**, *38* (11−12), 913−923.

(6) Prato, M. Fullerenes And Related Structures. In *Topics In Current Chemistry*; Springer-Verlag: Berlin, Germany, 1999; Vol. 199, pp 173−187.

(7) Subramoney, S. *Adv. Mater.* **1998**, *10* (15), 1157−1171.

(8) Degiorgi, L. *Adv. Phys.* **1998**, *47* (2), 207−316.

(9) Prato, M. *J. Mater. Chem.* **1997**, *7* (7), 1097−1109.

(10) Ball, P. *Nature* **2001**, *414* (6860), 142−144.

(11) Endo, M.; Hayashi, T.; Kim, Y. A.; Terrones, M.; Dresselhaus, M. S. *Philos. Trans. R. Soc. London, Ser. A* **2004**, *362*, 2223−2238.

(12) Violi, A. *Combust. Flame* **2004**, *139* (4), 279−287.

(13) Violi, A.; Sarofim, A. F.; Voth, G. A. *Combust. Sci. Technol.* **2004**, *176* (5−6), 991−1005.

(14) Violi, A.; Voth, G. A.; Sarofim, A. F. *Proc. Combust. Inst.* **2005**, *30*, 1343−1351.

(15) Colvin, V. L. *Nat. Biotechnol.* **2003**, *21* (10), 1166−1170.

(16) Sayes, C. M.; Fortner, J. D.; Guo, W.; Lyon, D.; Boyd, A. M.; Ausman, K. D.; Tao, Y. J.; Sitharaman, B.; Wilson, L. J.; Hughes, J. B.; West, J. L.; Colvin, V. L. *Nano Lett.* **2004**, *4* (10), 1881−1887.

(17) Warheit, D. B.; Laurence, B. R.; Reed, K. L.; Roach, D. H.; Reynolds, G. A. M.; Webb, T. R. *Toxicol. Sci.* **2004**, *77* (1), 117−125.

(18) Lam, C. W.; James, J. T.; McCluskey, R.; Hunter, R. L. *Toxicol. Sci.* **2004**, *77* (1), 126−134.

(19) Shvedova, A. A.; Castranova, V.; Kisin, E. R.; Schwegler-Berry, D.; Murray, A. R.; Gandelsman, V. Z.; Maynard, A.; Baron, P. *J. Toxicol. Environ. Health, Part A* **2003**, *66* (20), 1909−1926.

(20) Huczko, A.; Lange, H.; Calko, E.; Grubek-Jaworska, H.; Droszcz, P. *Fullerene Sci. Technol.* **2001**, *9* (2), 251−254.

(21) Huczko, A.; Lange, H.; Calko, E. *Fullerene Sci. Technol.* **1999**, *7* (5), 935−939.

(22) Maynard, A. D.; Baron, P. A.; Foley, M.; Shvedova, A. A.; Kisin, E. R.; Castranova, V. *J. Toxicol. Environ. Health, Part A* **2004**, *67* (1), 87−107.

(23) Service, R. F. *Science* **2005**, *310*, 1609−1609.

(24) Arnall, A. H. *Future Technologies, Today's Choices*; Greenpeace Environmental Trust: London, 2003.

(25) Dockery, D. W.; Pope, C. A.; Xu, X.; Spengler, J. D.; Ware, J. H.; Fay, M. E.; Ferris, B. G.; Speizer, F. E. *N. Engl. J. Med.* **1993**, *329* (24), 1753.
(26) *HEI Special Report: Research Directions to Improve Estimates of Human Exposure and Risk from Diesel Exhaust*; Health Effects Institute: Boston, MA, 2002.
(27) Oberdörster, G.; Ferin, J.; Lehnert, B. E. *Environ. Health Perspect.* **1994**, *102* (S5), 173−179.
(28) Hansen, J.; Nazarenko, L. *Proc. Natl. Acad. Sci. U.S.A.* **2004**, *101*, 423−428.
(29) Merlo, D. F.; Garattini, S.; Gelatti, U.; Simonati, C.; Covolo, L.; Ceppi, M.; Donato, F. *Occup. Environ. Med.* **2004**, *61* (2).
(30) Uragoda, C. G. *Occup. Med.* **1997**, *47* (5), 269−272.
(31) Adelmann, P., Baierl, T., Drosselmeyer, E., Politis, G., Seidel, A., Schwegler-Berry, D., Steinleitner, G., Eds. Effects of fullerenes on alveolar macrophages in vitro. In *Toxic and Carcinogenic Effects of Solid Particles in the Respiratory Tract*; ILSI Press: Washington, DC, 1994.
(32) Saiz, L.; Bandyopadhyay, S.; Klein, M. L. *Biosci. Rep.* **2002**, *22* (2), 151−173.
(33) Redondo, A.; LeSar, R. *Annu. Rev. Mater. Res.* **2004**, *34*, 279−314.
(34) Voth, G. A. *Front. Biosci.* **2003**, *8*, S1384−S1397.
(35) Schlick, T.; Barth, E.; Mandziuk, M. *Annu. Rev. Biophys. Biomol. Struct.* **1997**, *26*, 181−222.
(36) Kohl, P.; Noble, D.; Winslow, R. L.; Hunter, P. J. *Philos. Trans. R. Soc. London, Ser. A* **2000**, *358* (1766), 579−610.
(37) Moraitakis, G.; Purkiss, A. G.; Goodfellow, J. M. *Rep. Prog. Phys.* **2003**, *66* (3), 383−406.
(38) Florian, J.; Goodman, M. F.; Warshel, A. *Proc. Natl. Acad. Sci. U.S.A.* **2005**, *102* (19), 6819−6824.
(39) Warshel, A. *Proc. Natl. Acad. Sci. U.S.A.* **2005**, *102* (6), 1813−1814.
(40) Zhu, Z. W.; Schuster, D. I.; Tuckerman, M. E. *Biochemistry* **2003**, *42* (5), 1326−1333.
(41) Xie, Y. H.; Soh, A. K. *Mater. Lett.* **2005**, *59* (8−9), 971−975.
(42) Gao, H. J.; Kong, Y. *Annu. Rev. Mater. Res.* **2004**, *34*, 123−150.
(43) Noon, W. H.; Kong, Y. F.; Ma, J. P. *Proc. Natl. Acad. Sci. U.S.A.* **2002**, *99*, 6466−6470.
(44) Friedman, S. H.; DeCamp, D. L.; Sijbesma, R. P.; Srdanov, G.; Wudl, F.; Kenyon, G. L. *J. Am. Chem. Soc.* **1993**, *115*, 6506−6509.
(45) Friedman, S. H.; Ganapathi, P. S.; Rubin, Y.; Kenyon, G. L. *J. Med. Chem.* **1998**, *41* (13), 2424−2429.
(46) Yeh, I. C.; Hummer, G. *Proc. Natl. Acad. Sci. U.S.A.* **2004**, *101* (33), 12177−12182.
(47) Srinivas, G.; Klein, M. L. *Nanotechnology* **2004**, *15*, 1289−1295.
(48) Kittelson, D. B. *J. Aerosol. Sci.* **1998**, *29* (5−6), 575−588.
(49) Bagley, S. T.; Baumgard, K. J.; Gratz, L. D.; Johnson, J. J.; Leddy, D. G. *Research Report 76: Effects of Fuel Modification and Emission Control Devices on Heavy-Duty Diesel Engine Emissions*; Health Effects Institute, Boston, MA, 1996.
(50) Ristovski, Z. D.; Morawska, L.; Bofinger, N. D.; Hitchins, J. *Environ. Sci. Technol.* **1998**, *32* (24), 3845−3852.
(51) Goel, A.; Hebgen, P.; Vander Sande, J. B.; Howard, J. B. *Carbon* **2002**, *40*, 177−182.
(52) Goel, A.; Howard, J. B.; Vander Sande, J. B. *Carbon* **2004**, *42*, 1907−1915.
(53) Vander Wal, R. L.; Tomasek, A. J.; Pamphlet, M. I.; Taylor, C. D.; Thompson, W. K. *J. Nanopart. Res.* **2004**, *6*, 555−568.
(54) Smith, W.; Forester, T. R. *J. Mol. Graphics* **1996**, *14*, 136−141.
(55) Mayo, S. L.; Olafson, B. D.; Goddard, W. A., III. *J. Phys. Chem.* **1990**, *94*, 8897−8909.
(56) Ryckaert, J. P.; Ciccotti, G.; Berendsen, H. J. C. *J. Comput. Phys.* **1977**, *23*, 327−341.
(57) Smondyrev, A. M.; Berkowitz, M. L. *J. Comput. Chem.* **1999**, *20* (5), 531−545.
(58) Smondyrev, A. M.; Berkowitz, M. L. *J. Chem. Phys.* **1999**, *111* (21), 9864−9870.
(59) Smondyrev, A. M.; Berkowitz, M. L. *Biophys. J.* **1999**, *77* (4), 2075−2089.
(60) Smondyrev, A. M.; Berkowitz, M. L. *J. Chem. Phys.* **1999**, *110* (8), 3981−3985.
(61) Smondyrev, A. M.; Berkowitz, M. L. *Biophys. J.* **2000**, *78* (4), 1672−1680.
(62) Smondyrev, A. M.; Berkowitz, M. L. *Chem. Phys. Lipids* **2001**, *112* (1), 31−39.
(63) Smondyrev, A. M.; Berkowitz, M. L. *Biophys. J.* **2001**, *80* (4), 1649−1658.
(64) Smondyrev, A. M.; Voth, G. A. *Biophys. J.* **2002**, *82* (3), 1460−1468.
(65) Chang, R. W.; Ayton, G. S.; Voth, G. A. *J. Chem. Phys.* **2005**, *122*, 244716.
(66) Jorgensen, W. L.; Chandrasekhar, J.; Madura, J. D.; Impey, R. W.; Klein, M. L. *J. Chem. Phys.* **1983**, *79*, 926−935.
(67) Lindahl, E.; Edholm, O. *Biophys. J.* **2000**, *79* (1), 426−433.
(68) Marrink, S. J.; Mark, A. E. *J. Phys. Chem. B* **2001**, *105*, 6122−6127.
(69) Hofsäss, C.; Lindahl, E.; Edholm, O. *Biophys. J.* **2003**, *84* (4), 2192−2206.
(70) de Vries, A. H.; Mark, A. E.; Marrink, S. J. *J. Am. Chem. Soc.* **2004**, *126* (14), 4488−4489.
(71) Torrie, G. M.; Valleau, J. P. *J. Comput. Phys.* **1977**, *23*, 187−199.
(72) Roux, B. *Comput. Phys. Commun.* **1995**, *91*, 275−282.
(73) Steinfeld, J. I.; Francisco, J. S.; Hase, W. L. *Chemical Kinetics and Dynamics*, 2nd ed.; Prentice Hall: Upper Saddle River, NJ, 1998.
(74) Lipowsky, R., Sackmann, E., Eds. *Structure and Dynamics of Membranes*; Elsevier Science Pub Co.: Amsterdam, The Netherlands, 1995.
(75) Evans, E.; Rawicz, W. *Phys. Rev. Lett.* **1990**, *64* (17), 2094−2097.